



UNIVERSITY OF LEEDS

This is a repository copy of *Single Particle Cryo-Electron Microscopy: From Sample to Structure*.

White Rose Research Online URL for this paper:
<https://eprints.whiterose.ac.uk/175632/>

Version: Accepted Version

Article:

White, JBR, Maskell, DP, Howe, A et al. (5 more authors) (2021) Single Particle Cryo-Electron Microscopy: From Sample to Structure. *Journal of Visualized Experiments* (171). e62415. ISSN 1940-087X

<https://doi.org/10.3791/62415>

© 2021 JoVE Journal of Visualized Experiments. This is an author produced version of an article, published in *Journal of Visualized Experiments*. Uploaded in accordance with the publisher's self-archiving policy.

Reuse

Items deposited in White Rose Research Online are protected by copyright, with all rights reserved unless indicated otherwise. They may be downloaded and/or printed for private study, or other acts as permitted by national copyright laws. The publisher or other rights holders may allow further reproduction and re-use of the full text version. This is indicated by the licence information on the White Rose Research Online record for the item.

Takedown

If you consider content in White Rose Research Online to be in breach of UK law, please notify us by emailing eprints@whiterose.ac.uk including the URL of the record and the reason for the withdrawal request.



eprints@whiterose.ac.uk
<https://eprints.whiterose.ac.uk/>

1 **TITLE:**

2 **Single particle cryo-electron microscopy: From sample to structure**

3

4 **AUTHORS AND AFFILIATIONS:**

5 Joshua B. R. White¹, Daniel P. Maskell¹, Andrew Howe², Martin Harrow² Daniel K. Clare², C.
6 Alistair Siebert², Emma L. Hesketh¹, Rebecca F. Thompson⁺¹

7

8 ⁺ Corresponding author

9

10 ¹ Astbury Centre Structural Molecular Biology, School Molecular and Cellular Biology, Faculty
11 Biological Sciences, University of Leeds, Leeds, UK

12 ² Diamond Light Source, Harwell Science and Innovation Campus, Didcot, UK

13

14 Email addresses

15 JBRW- bsjw@leeds.ac.uk

16 RFT- r.f.thompson@leeds.ac.uk

17 ELH- E.L.Hesketh@leeds.ac.uk

18 DPM- d.p.maskell@leeds.ac.uk

19 AH-Andrew.Howe@diamond.ac.uk

20 MH-Martin.Harrow@diamond.ac.uk

21 DKC-Daniel.Clare@diamond.ac.uk

22 CAS-Alistair.Siebert@diamond.ac.uk

23

24 **KEYWORDS:**

25 CryoEM, single particle, structure, electron microscopy

26

27 **SUMMARY:**

28 Structure determination of macromolecular complexes using cryoEM has become routine for
29 certain classes of proteins and complexes. Here, this pipeline is summarized (sample preparation,
30 screening, data acquisition and processing) and readers are directed towards further detailed
31 resources and variables that may be altered in the case of more challenging specimens.

32

33 **ABSTRACT:**

34 Cryo-electron microscopy (cryoEM) is a powerful technique for structure determination of
35 macromolecular complexes, via single particle analysis (SPA). The overall process involves i)
36 vitrifying the specimen in a thin film supported on a cryoEM grid; ii) screening the specimen to
37 assess particle distribution and ice quality; iii) if the grid is suitable, collecting a single particle
38 dataset for analysis; and iv) image processing to yield an EM density map. In this protocol, an
39 overview for each of these steps is provided, with a focus on the variables which a user can
40 modify during the workflow and the troubleshooting of common issues. With remote microscope
41 operation becoming standard in many facilities, variations on imaging protocols to assist users in
42 efficient operation and imaging when physical access to the microscope is limited will be
43 described.

44

45 INTRODUCTION:

46 Single particle CryoEM

47 To investigate life at a molecular level we must understand structure. Many techniques to probe
48 protein structure are available, such as NMR, X-ray crystallography, mass spectrometry and
49 electron microscopy (EM). To date, the majority of structures deposited to the Protein Databank
50 (PDB) have been solved using X-ray crystallography. However, from ~2012 onwards, cryo-
51 electron microscopy (cryoEM) became a mainstream technique for protein structure
52 determination and its use increased dramatically. The total number of EM maps deposited to the
53 Electron Microscopy Databank (EMDB) (as of Dec 2020) was 13,421 compared with 1,566 in 2012
54 (Figure 1, www.ebi.co.uk). In 2012 the number of atomic coordinates modelled in cryoEM density
55 maps, deposited to the PDB was just 67 but as of Dec 2020, 2,309 structures have been deposited
56 so far, a 35-fold increase. This underlying growth in the quality and quantity of cryoEM density
57 maps produced, sometimes referred to as the 'resolution revolution'¹, was caused by a
58 coalescence of advances in multiple areas: the development of new cameras for imaging known
59 as direct electron detectors; new software; and more stable microscopes²⁻⁴.

60
61 [Place Figure 1 here]

62
63 Single particle analysis (SPA) is a powerful tool to generate biological insight in a wide variety of
64 sample types by elucidating high resolution structures of isolated complexes^{5, 6} including viruses^{7,}
65 ⁸, membrane proteins^{9, 10}, helical assemblies¹¹ and other dynamic and heterogeneous
66 macromolecular complexes^{12, 13}, the sizes of which vary by orders of magnitude (from 39 kDa^{14,}
67 ¹⁵ to tens of megadaltons). Here, a protocol for a standard pipeline for cryoEM SPA from sample
68 to structure is described.

69
70 Prior to embarking upon this pipeline, a purified sample should be subjected to biochemical
71 analysis to assess its chances of downstream success. Preparation of a suitable sample is arguably
72 the biggest barrier to SPA, particularly for transient and heterogeneous (both compositional and
73 conformational) complexes. The macromolecular complex preparation should contain as few
74 contaminants as possible, at sufficient concentration to yield many particles in each cryoEM
75 micrograph, and in a buffer composition well suited to cryoEM analysis. Certain buffer
76 constituents, including sucrose, glycerol and high (~> 350 mM concentrations of salts, depending
77 on the sample size, properties and other buffer constituents) can interfere with the process of
78 vitrification or reduce the signal-to-noise ratio in images, hindering structure determination¹⁶.

79
80 Typically, as a minimum, size exclusion chromatography (SEC) and SDS- PAGE gel analysis should
81 be used to assess sample purity^{17, 18}, but circular dichroism, functional assays, SEC coupled with
82 multi-angle light scattering, and thermal stability assays are all useful tools for qualitative analysis
83 of macromolecular complex preparations prior to cryoEM analysis. However, the results from
84 these biochemical analyses may yield little insight into the structural heterogeneity of the sample
85 and its behaviour on a cryoEM grid. For this reason, negative stain EM is routinely used as a quick,
86 cheap and powerful tool for assessing compositional and conformational heterogeneity, and
87 therefore a good way of ascertaining which elution fraction from a purification is most promising,
88 or screening different buffer compositions^{19, 20}. Once a promising sample has been identified, we

89 can proceed to the SPA cryoEM pipeline. Negative stain does not always align with the
90 subsequent results seen in cryoEM; sometimes a sample looks poor by negative stain but
91 improves when seen in vitreous ice in cryoEM. In contrast, sometimes samples look excellent
92 during negative stain steps but require significant further optimisation when progressing to
93 cryoEM. However, in the majority of cases negative stain provides a useful quality control step.

94

95 **Vitrification**

96 The harsh environment within the vacuum system of the electron microscope causes both
97 dehydration and radiation damage to unfixed biological specimens²¹. Therefore, to image the
98 sample in a native-like state, the biological specimen must be preserved prior to imaging. For
99 purified preparations of macromolecular complexes, vitrification is the method of choice to
100 enable its visualization by cryoEM whilst preserving the atomic details of the complex. The
101 discovery of vitrification as a method of sample preparation was a fundamental advancement in
102 electron microscopy of biological specimens, for which Dubochet was recognized in the 2017
103 Nobel Prize in Chemistry. Sample vitrification involves creating a thin layer of solution containing
104 the specimen of interest, typically tens of nm thick, suspended on a cryoEM grid support. The
105 thin film is then frozen extremely rapidly in a cryogen such as liquid ethane at ~ -175 °C. The
106 freezing rate is $\sim 10^6$ °C/s, fast enough that amorphous, or vitreous ice forms, suspending the
107 specimen in a thin, solid film²².

108

109 The initial variable to consider is the cryoEM grid support chosen²³. An EM grid typically consists
110 of an amorphous carbon film with perforations (either regular or irregular), over a support
111 structure. The support structure is typically a circular metal grid 3.05 mm in diameter, usually
112 made from copper, but other metals such as gold, or molybdenum (which has preferred thermal
113 expansion properties²⁴) can be used. Sometimes, an additional thin, continuous support is
114 applied across the grid, such as graphene, graphene oxide or a thin ($\sim 1-2$ nm) amorphous carbon
115 layer. While standard cryoEM grids (most commonly 400-200 mesh copper with a perforated (1.2
116 μm round holes separated by 1.3 μm (r1.2/1.3), or 2 μm separated by 2 μm of carbon (r2/2))
117 carbon support- although many different patterns are available) have been used in the vast
118 majority of structures reported to date, novel grid technologies with improved conductivity and
119 reduced specimen movement have been reported²⁵. Selected grids are subjected to a glow-
120 discharge/plasma cleaning treatment to render them hydrophilic and amenable to sample
121 application²⁶.

122

123 Following glow-discharge, the next stage is thin film formation. This thin film is most commonly
124 formed using filter paper to remove excess liquid from the grid. While this can be carried out
125 manually, a number of plunge freezing devices are commercially available, including the Vitrobot
126 Mk IV (Thermo Fisher Scientific), EM GP II (Leica) and CP3 (Gatan). With these devices, $\sim 3-5$ μL of
127 sample in solution is applied to the EM grid, followed by blotting away excess solution using filter
128 paper. The grid, with a thin film suspended across it, is then plunged into liquid ethane cooled by
129 liquid nitrogen (LN_2) to ~ -175 °C. Once frozen, the grid is maintained at a temperature below the
130 devitrification point (-137 °C) prior to, and during imaging.

131

132 **Specimen screening and data collection**

133 Following vitrification of a cryoEM grid, the next stage is to screen the grid to assess its quality
134 and to determine whether the grid is suitable to proceed to high resolution data collection. An
135 ideal cryoEM grid has vitreous ice (opposed to crystalline ice) with the ice thickness just sufficient
136 to accommodate the longest dimension of the specimen, ensuring the surrounding ice
137 contributes as little noise to the resulting image as possible. The particles within the ice should
138 have a size and (if known) shape consistent with biochemistry, and ideally be monodisperse with
139 a random distribution of particle orientations. Finally, the grid should have enough areas of
140 sufficient quality to satisfy the desired data collection length. Depending on the specimen, this
141 may take many iterations of vitrification and screening until optimal grids are produced. Both
142 fortunately and unfortunately, there are a huge range of variables that can be empirically tested
143 to alter particle distribution on cryoEM grids (reviewed in^{16,27}). In this manuscript, representative
144 results for a membrane protein project¹⁰ are shown.

145
146 Once a suitable grid has been identified, data collection can proceed. Several models of cryo-
147 transmission electron microscopes for biological specimens are optimized to collect high-
148 resolution data in an automated fashion. Typically, data is collected on 300 kV or 200 kV systems.
149 Automated data collection can be achieved using software including EPU (Thermo Fisher
150 Scientific)²⁸, Legion²⁹, JADAS³⁰ and SerialEM^{31, 32}. An automated data collection with modern
151 detectors typically results in terabytes (TB) of raw data in a 24 h period (average datasets are ~ 4
152 TB in size).

153
154 Due to the COVID-19 restrictions in place on much of the world (time of writing December 2020),
155 many microscopy facilities have moved to offering remote access. Once the grids have been
156 loaded into the autoloader of a microscope, data acquisition can be conducted remotely.

157
158 **Image processing and model building**

159 Where a data collection session may be typically 0.5-4 days, subsequent image processing may
160 take many weeks and months, depending on the availability of computing resources. It is
161 standard for initial image processing steps, namely motion correction and contrast transfer
162 function (CTF) estimation to take place 'on the fly'^{33,34}. For downstream processing, there are a
163 plethora of software suites available. Particles are 'picked' and extracted from micrographs^{35, 36}.
164 Once particles are extracted, a standard protocol would be to process the particles through
165 several rounds of classification (in both two dimensions (2D) and three dimensions (3D) and/or
166 focused on specific regions of interest) to reach a homogeneous subset of particles. This
167 homogeneous subset of particles is then averaged together to produce a 3D reconstruction. At
168 this point data is often corrected further to produce the highest quality map possible, for example
169 through CTF refinement, distortion corrections³⁷ and Bayesian polishing³⁸. The outcome of this
170 image processing is a 3D cryoEM map of the biological specimen of interest. The resolution range
171 reached in a 'standard' automated single particle experiment from a grid of sufficient quality,
172 with data collected on a 300 kV microscope system is typically between 10 Å and 2 Å depending
173 on the size and flexibility of the protein complex. With an ideal specimen, resolutions of ~1.2 Å
174 have now been reached using SPA workflows⁵. While this protocol details steps towards
175 obtaining an EM density map, once this is in hand it can be further interpreted through fitting
176 and refining a protein model (if resolution is < 3.5 Å) or building *de novo*³⁹. Data associated with

177 structure determination experiments can be deposited into online public repositories, including
178 EM density maps (Electron Microscopy Data Bank)⁴⁰, resulting atomic coordinates (Protein Data
179 Bank)⁴¹ and raw datasets (Electron Microscopy Public Image Archive)⁴².

180

181 In this protocol, the outer-membrane protein complex RagAB (~340 kDa) from *Porphyromonas*
182 *gingivalis* is used as an example macromolecular complex¹⁰ (EMPIAR-10543). For those new to
183 cryoEM, support for samples through this pipeline from sample to structure is available, subject
184 to peer review, through funded access schemes such as iNEXT Discovery and Instruct.

185

186 **PROTOCOL:**

187

188 **1. Grid Vitrification**

189

190 NOTE: For all steps in steps 1 and 2, ensure that all tools are clean, dry and at room temperature
191 before cooling them to LN₂ temperature, using freshly decanted LN₂ to reduce ice contamination.
192 Where possible, work within a humidity-controlled environment with < 20% relative humidity.
193 Ensure appropriate personal protective equipment and H&S documentation is in place before
194 commencing work.

195

196 1.1. Ensure the specimen of interest is ready for sample preparation.

197

198 1.2. Choose appropriate cryoEM grids and ensure these have been rendered hydrophilic using
199 glow discharge or plasma treatment. A wide variety of systems and variations to the protocol are
200 available but all involve placing the grids into a glow discharge/plasma cleaning system and
201 running a program which will pump the chamber to a desired vacuum level, before introducing a
202 specific gas mixture/chemical vapor or air into the system. An electric current is passed through
203 the system, ionizing the gas particles and inducing the surface of the grids to be rendered more
204 hydrophilic.

205

206 1.3. Start up the plunge freezing device for grid vitrification by turning on the system using the
207 power switch on the back, and wait for the touch screen to load.

208

209 1.4. Using the provided stylus or fingers, in **Console**, set the desired working temperature of
210 the chamber (range available is 4 – 60 °C, recommended for most macromolecules 4-6 °C).

211

212 1.5. Fill the humidifier with 50 mL of type II lab water using a syringe, via the rubber tubing at
213 bottom of humidifier. Making sure to remove any trapped air in the syringe prior to filling. Be
214 careful not to overfill the humidifier or water will exude into the chamber. Once the humidifier
215 is filled, draw back the syringe plunger by 5-10 mL to create a vacuum seal.

216

217 1.6. In **Console**, set the desired relative humidity for the chamber (range available is 0-100%,
218 humidity of 95-100% is typically used). Leave humidity set to 'off' until immediately prior to grid
219 making so that the chamber does not get too wet.

220

221 1.7. Obtain the plunge freezing device tweezers and filter paper cut to the correct size to fit
222 onto the pads, either purchased or using a stamp to cut an aperture of the appropriate size.

223

224 1.8. Prepare the cryogen for plunge freezing.

225

226 1.8.1. Place the metal cryo-grid box holder, cryogen cup and metal spider's legs into the coolant
227 container.

228

229 1.8.2. Cool down the container by filling up the outer chamber with LN₂. Keep the outer
230 chamber topped up to cover the top of the cryo-grid box holder. Add ~ 1 cm of additional LN₂ to
231 the cryogen cup to assist equilibration of the system to LN₂ temperature.

232

233 NOTE: The anti-contamination ring can be used to limit humid air condensing around the cryogen
234 cup and leading to cryo-coolant/ethane contamination. This is not generally required in a
235 humidity-controlled environment. If using the anti-contamination ring, be careful not to overfill
236 the container with LN₂ or it may spill when the ring is pressed into the container later in the
237 process.

238

239 1.8.3. Wait 3-5 min to observe the boiling of the spider legs, and then wait a further 3 min to
240 ensure the cryogen cup is sufficiently cold to condense the vitrification medium.

241

242 1.9. Liquefy the cryogen (liquid ethane) into the cryogen cup.

243

244 1.9.1. Take the ethane cylinder pipe with thin tubing and a nozzle to dispense the gas. A P200
245 pipette tip with the aperture opened by cutting off the very tip using a razor blade is ideal here.
246 A wider aperture is needed to prevent ethane solidifying at the tip and blocking the flow of gas.

247

248 1.9.2. Ensuring the cryogen cup does not contain any remaining LN₂, take the ethane gas nozzle
249 and place it within the cryogen cup. Using the gas cylinder regulator, start a low flow and dispense
250 cryogen gas into the cryogen cup to condense the gas. Keep the tip from which the gas flows
251 directly pressed against the wall of the cryogen cup but move it gently back and forth in a tapping
252 motion against the surface. Regulate the flow of the gas to allow a low, steady flow to begin to
253 condense/liquify in a controlled fashion within the cryogen cup.

254

255 1.9.3. Fill the cup to just below the silver spider rim and stop the gas flow, then remove gas line
256 carefully to avoid contaminating the surrounding LN₂ with ethane.

257

258 1.9.4. Top up the coolant container with LN₂, being very careful not to spill any into the liquid
259 ethane.

260

261 1.9.5. Leave the spiders legs in position for ~ 3-5 min to ensure the liquid ethane is equilibrated
262 to a sufficiently cold temperature. The cryogen will begin to look cloudy/slightly opaque. This
263 indicates that it is close to its freezing point. At this stage, use tweezers to remove the spider. As
264 long as the LN₂ is kept within the container surrounding the cryogen cup, the ethane will now

265 stay liquefied and suitable for vitrification for 1-2 h. However, aim to complete the procedure as
266 quickly as possible, especially in non-humidity-controlled rooms, to reduce ice contamination.

267
268 NOTE: If the spider appears to be 'stuck on', use a metal object such as a nut and hold against the
269 spider's legs to warm them up slightly, and then remove the legs.

270
271 1.10. Prepare the plunge freezing device and accessories for sample vitrification.

272
273 1.11. Add grid storage boxes to the metal cryo-grid box holder and throughout the procedure
274 ensure the LN₂ is kept topped up to just above the level of the grid boxes (usually every ~ 5 min).

275
276 1.12. On the plunge freezing device screen, in the **Process Parameters** box input the chosen
277 parameters including: blot time (the time the plunge freezing device pads will come together),
278 force (the distance of the blotting pads from the grid, which alters the gradient of ice formation)
279 and total (number of times the blotting pads will come in to meet). Choose these parameters
280 based on the individual plunge freezing device and behaviour of the macromolecule. Typical
281 values are a blot force between 0 and 5, blot time from 1-6 s and a blot total of 1. Typical wait
282 time (time between initiating the blot, and the blot beginning) and drain time (time after blotting
283 before plunging) is 0-2 s.

284
285 NOTE: Depending on user preferences, additional options in the **Options, Miscellaneous** section
286 can be selected, including **Use Foot Pedal** to move to the next step on each press, **Skip grid**
287 **transfer** (skips the final step where the tweezer arm is raised slightly), turn **Humidity off during**
288 **process** (while the sample is being applied, stops active humidification of the chamber which can
289 make it harder to see the grid) and **Autoraise ethanelift** (combines the step of tweezers being
290 raised into the chamber and raising the coolant container- skips **Raise ethane container** step).
291 Here, all of these options are turned on.

292
293 1.13. Place the coolant container securely onto the moving platform arm under the chamber

294
295 1.14. Insert fresh blotting paper onto each blotter arm making sure plastic ring clips are
296 secured. Each filter paper will allow 16 blots (arms rotate blotting paper). Press the **Reset Blot**
297 **Paper** button in **Controls** section.

298
299 1.15. Run 1 full cycle of the plunge freezing device vitrification process to ensure that each
300 moving part is behaving as expected.

301
302 1.15.1. Press (or use foot pedal) to **Place New Grid**, then **Start Process**, then **Process** then
303 **Continue**. At this stage, watch to ensure the blotting arms are contacting each other as expected.

304
305 1.16. Turn 'on' the humidifier. Water vapor will be produced (as long as the set humidity is
306 higher than currently in the chamber).

307
308 1.17. The specimen of interest can now be vitrified. Use the foot pedal or **Place New Grid** and

309 the plunging rod will descend out of the chamber allowing the tweezers to be attached into the
310 mount.

311

312 1.17.1. Using the plunge freezing device tweezers, pick up the desired glow discharged/plasma
313 cleaned cryoEM grid, taking care to note which side is the correct side to be used for sample
314 application according to the grid manufacturer. Pick up the grid by the rim, taking care to avoid
315 excessive/unnecessary contact with the tweezers as this will damage the support. Secure the grid
316 in the tweezers by moving the black clip down to the ridged part of the tweezers. The grid needs
317 to be securely held, but the clip should not be too far down as it will contact the blotting pads,
318 leading to irreproducible blotting and, later, the tweezers will need to be held below this point
319 when releasing the clip.

320

321 1.17.2. Place the plunge freezing device tweezers holding the cryoEM grid onto the pneumatic
322 arm with the correct side facing your dominant hand. The design of the plunge freezing device
323 tweezers and chamber are such that the sample can be applied through either the right or left-
324 hand side of the chamber, according to the handedness of the user.

325

326 NOTE: Applying the sample on different sides with the same blotting parameters rarely results in
327 comparable results, so left-handed researchers may need to tune their blotting parameters
328 independently of their right-handed colleagues.

329

330 1.17.3. Press **Start Process** and the grid held in the tweezers will be taken into the chamber and
331 the coolant container will be raised.

332

333 1.17.4. Press **Process** and the tweezers will move the grid to the position where a pipette can be
334 used to apply the specimen to the grid. Open the side port facing the correct side of the grid and
335 apply sample by pipetting, making sure that the pipette tip does not touch the grid as it may lead
336 to damage of the grid support/bending the grid, but dispense the liquid close enough so that the
337 droplet dispenses onto the grid. Typically, 3-5 μL is applied.

338

339 1.18. Press **Continue** and user predefined parameters will blot the grid and then plunge the
340 tweezers with grid mounted into the coolant cup for sample vitrification. Tweezers will descend
341 in conjunction with the arm holding the coolant container and coolant, keeping the grid
342 submerged in the cryogen.

343

344 1.19. Transfer the grid from the cryogen cup to the grid storage box submerged in LN_2 .

345

346 1.19.1. Detach the tweezers from the tweezer arm, taking great care not to contact the vitrified
347 grid with the sides of the cryogen cup. Adjust the grip so that the tweezers are held comfortably.
348 As quickly and carefully as possible, move the grid from the cryogen to the LN_2 . With one hand,
349 hold the tweezers shut using your fingers and with the other hand, slide the black clip upwards
350 out of the way, holding the tweezers shut. Readjust the grip and manipulate the grid into the grid
351 storage box.

352

353 1.19.2. Repeat steps 1.10-1.19 until all grids are made (a typical session will involve making 4-12
354 grids). Store all grid storage boxes containing grids in LN₂ dewar until the next stages.

355

356 **2. Clipping grids for loading into an autoloader microscope**

357

358 2.1. Clip grids into autogrid assembly according to the protocol previously described ²⁸.

359

360 **3. Secure remote log in to microscopes**

361

362 NOTE: With COVID-19 controls at the time of writing, but also with environmental concerns
363 associated with international travel, more microscopy facilities have been offering services where
364 the user operates remotely. The method of implementation for this will vary according to the
365 local IT configuration of each facility, and the needs of its internal and external user community.
366 Here the process for remotely accessing cryoEMs at eBIC and controlling the microscope through
367 EPU software is described.

368

369 3.1. Remotely log in to cryoEM's. Remote logon is mediated via NoMachine software to access
370 the microscope support PC and is configured to only allow access to users who are registered on
371 a visit via the users FedID logon credentials. Access remains active only for the duration of the
372 session.

373

374 3.2. Open NoMachine and start a new NX connection to nx-cloud.diamond.ac.uk with
375 password authentication.

376

377 3.3. Open the connection and log in with the username *fedid@fed.cclrc.ac.uk* and FedID
378 password. Double-click the icon corresponding to relevant microscope from the available options
379 to open a connection to the relevant support PC.

380

381 3.4. Enter username *clrc\FedID* and password at the Windows logon screen.

382

383 3.5. Open TeamViewer software from the desktop icon and connect to PartnerID: TEM with
384 the supplied password. This establishes the connection from the support PC to the TEM PC. The
385 **Next Monitor** button in the TeamViewer ribbon can be used to toggle between the microscope
386 user interface and the EPU window.

387

388 3.6. Microscope functions can then be controlled by users directly through the EPU interface.

389

390 **4. Loading samples into an autoloader microscope and screening for ice and sample** 391 **quality**

392

393 NOTE: In this section a microscope with an autoloader and EPU software is used for sample
394 screening, but this can be achieved using other software and a side entry system and cryoEMs
395 from other manufacturers.

396

397 4.1. Load clipped grids into the microscope autoloader as previously described²⁸.
398

399 4.2. In the autoloader tab of the microscope user interface, tab out the **Options** dialogue using
400 the arrow and press the **Inventory** button. This will sequentially check each position in the
401 cassette to determine if a cartridge is present. Occupied slots will be labelled in blue. If all
402 occupied slots have been mapped, press the **Inventory** button again to stop after the current
403 position, otherwise leave running until all occupied slots have been mapped. Label all occupied
404 slots with the sample details in the boxes provided.
405

406 4.3. Highlight the grid to be transferred to the microscope column and click **Load**. The slot
407 label will turn from blue to yellow once the grid has been successfully loaded onto the stage.
408 Proceed to screen the grids.
409

410 4.3.1. Open EPU software. On the **Preparation** page, select **Acquisition optics and settings** then
411 select the **Atlas** preset from the drop-down menu. Choose appropriate beam setting presets
412 (e.g., 64x nominal mag, spot size 5, Microprobe, with an illuminated area in the parallel range for
413 Falcon detector- for further information choosing beam setting presets see²⁸). Press **Set** to push
414 the parameters to the microscope.
415

416 4.3.2. Press **Open column valves** and insert the FluScreen. Check that a beam is visible and
417 sufficiently spread and centered to cover the detector. If necessary, navigate to a thinner region
418 of the grid using the joystick or stage menu to control stage movements in X and Y.
419

420 4.3.3. Lift the FluScreen and take an image using the **Preview** button in EPU. Based on the
421 acquired image, the dose can be increased by moving to a lower number spot size, and vice versa.
422

423 4.3.4. In **EPU**, go to the **Atlas** page and press **New Session**. Select MRC image format and enter
424 a suitable folder name and location for saving the screening session, then click **Apply**.
425

426 4.3.5. Select **Screening** from the menu on the left. Tick the checkboxes next to each grid to have
427 an atlas montage acquired. **Start** the screening session in EPU. An atlas will be acquired for each
428 checked grid, with a number of available grid squares listed upon completion. Each atlas can be
429 viewed by highlighting it on the screening page, complete with a mark-up showing grid squares
430 with a similar predicted ice thickness grouped by colour.
431

432 4.4. On completion, review the collected atlases and identify the grids suitable for assessing
433 sample quality at higher magnifications (i.e., those with an appropriate number of grid squares
434 which are neither dry nor obscured by thick ice). Highlight the chosen grid on the EPU screening
435 menu and click **Load sample**.
436

437 4.4.1. Use the beam setting presets (See ²⁸ for explanation of beam setting presets desired for
438 each stage) and the preview function to examine the desired grid squares in greater detail.
439

440 4.4.2. From the Atlas screening menu, select the grid presently loaded and move the stage to a

441 grid square containing filled holes by right clicking over the desired location on the grid image
442 and selecting move to grid square.

443

444 4.4.3. Return to **EPU, Preparation** page and select the **GridSquare** preset.

445

446 4.4.4. Open the **EPU, Auto Functions** page and run **Auto-eucentric by stage tilt** with the
447 **GridSquare** preset to move the sample to eucentric height.

448

449 NOTE: **Auto-eucentric by beam tilt** is also available, which is faster but typically less accurate
450 than auto-eucentric by stage tilt.

451

452 4.4.5. In **EPU, Preparation**, take a new GridSquare **Preview** image. Note the differing grey
453 values across different holes indicating differing ice thicknesses. Move the stage over a hole using
454 **right click > move stage here**. Select the **Hole/Eucentric Height** preset and **Preview**.

455

456 NOTE: Depending on the molecular weight and shape of the particle of interest, it may be
457 possible to identify it at Hole/Eucentric Height magnification.

458

459 4.4.6. Select **Data Acquisition** preset and set a magnification that allows easy identification of
460 the particles (corresponding to an object sampling of generally $<2 \text{ \AA}/\text{pixel}$). Set the defocus offset
461 to ~ -3 to -5 \mu m with an exposure electron dose of $\sim 40\text{-}80 \text{ e}^-/\text{\AA}^2$.

462

463 4.5. Iterate through steps 4.3-4.4 to assess a range of ice thicknesses for particle distribution,
464 orientation and contamination across the grid. The particle distribution may vary close to the
465 edges versus the center of the hole and hence it is important to survey different locations with
466 the hole.

467

468 4.6. Screen all grids which show promise from atlases as having sufficient grid squares. Either
469 keep these in the microscope and proceed to data acquisition using EPU, or unload the samples
470 from the microscope and store under LN_2 until data collection is scheduled.

471

472 **5. Single particle cryoEM data collection (with a focus on remote operation)**

473

474 NOTE: A detailed protocol for data acquisition with EPU is described in the manufacturers manual
475 and elsewhere²⁸. Here modifications of this protocol for remote operation (namely reducing use
476 of the hand panels to conduct tasks and using software-based alternatives) are highlighted.

477

478 5.1. Unless one has already been collected during the session, collect an Atlas for the grid.

479

480 5.2. Define each of the beam setting presets according to the experimental needs of the
481 project.

482

483 5.3. Perform image shift calibrations²⁸.

484

485 5.4. Set up the EPU session.
486
487 5.4.1. In **EPU**, select **EPU** page then **Session Setup**, select **New session** then **New from**
488 **preferences**.
489
490 5.4.2. Select **New session** a pop up will appear providing an option to use previous settings. **Yes**
491 will automatically load the settings from the previous EPU (i.e., specimen carrier, defocus range,
492 autofocus settings, grid type) into the current EPU session. Selecting **'New from preferences'**
493 enables the user to pick a file with saved preferences (i.e., defocus range, autofocus settings, grid
494 type) and this information will be preloaded into EPU.
495
496 5.4.3. Fill in session name with something informative. The local facility may suggest a naming
497 convention.
498
499 5.4.4. In **Type**, select **Manual**.
500
501 5.4.5. For **Acquisition mode**, select **accurate hole centering** or **faster acquisition**.
502
503 5.4.6. In Image format select desired format.
504
505 5.4.7. Select an appropriate **Storage Folder** and EPU will create a directory with the session
506 name.
507
508 5.4.8. Select the appropriate **Specimen Carrier** according to which grid type and hole spacing
509 being used (e.g., Quantifoil 1.2/1.3) and press **Apply**. This protocol describes the process for
510 generating a template for a regular array of holes
511
512 5.5. Select an initial grid square and set an acquisition template.
513
514 5.5.1. Go **Square selection**, if all squares are green, click unselect all in top left.
515
516 5.5.2. Open tiles (**right click > open tile**). Select a square (**right click > add, right click > Move**
517 **stage to grid square**).
518
519 5.5.3. Go to **Hole selection** and press **Auto Eucentric**. Wait until this is complete and a Grid
520 Square image has been taken. If the autofunction fails this may be because the height is
521 significantly off, if so it can be adjusted manually using the FluScreen at Grid Square
522 magnification.
523
524 5.5.4. Measure hole size. Move and adjust the yellow circles so they are over the holes with
525 correct size and spacing.
526
527 5.5.5. Press **Find holes**. Check that the holes have been found correctly. If not change the hole
528 size and find holes again. Repeat this until it finds the hole correctly. If it consistently fails,

529 consider moving to a lower number (brighter) spot size at grid square magnification.
530

531 5.5.6. Use the **Filter ice quality** histogram on the right to adjust hole selection. This can be useful
532 to exclude areas with thick ice and thin ice. This will be remembered for future grid squares
533 selected during this session.
534

535 5.5.7. Optimize hole selection with the tools in **Select** menu at the top. For example, click
536 **Remove holes close to grid bar**.
537

538 5.5.8. Go to **Template definition** and press **Acquire**.
539

540 5.5.9. Click **Find and centre hole**. There will now be an image of a hole with a yellow circle
541 around the hole.
542

543 NOTE: If it struggles to find the hole, insert the objective aperture. If it still cannot find the hole,
544 try increasing the exposure time for the hole/eucentric height preset or increasing the defocus
545 for this preset or bin the image. A large defocus change may alter the image shift alignment.
546

547 5.5.10. Change the **Delay after Stage Shift** and the **Delay after Image Shift** times to 1-5 s.
548

549 5.5.11. Check **Maximum Image shift** value (if option is available) is as desired. If aberration free
550 image shift collection is being used, this value is defined in the EPU configuration file, otherwise
551 5 μm is a standard value.
552

553 5.5.12. Click **Add acquisition area**, then click anywhere on the image. Move the acquisition area
554 to desired location (i.e., at the edge of a hole) so that areas of acquisition are not doubly exposed
555 with the beam (The square in the green circle represents the detector area, the green circle is
556 the beam diameter).
557

558 5.5.13. On the top right, add the defocus range. Then add other acquisition areas. A typical
559 defocus list for a membrane protein project is -0.8 to -3 μm defocus.
560

561 5.5.14. Click **Add autofocus area** and click anywhere on the image. Move the autofocus area to
562 the carbon surrounding a hole. Standard practice is to autofocus after centring when using AFIS,
563 or every 5-15 μm , depending on the z-height variation across the square.
564

565 5.5.15. Click **Add drift measurement area**, drift measurement performed once per grid square,
566 with a set threshold of 0.05 nm/s is a standard setting. The drift measurement area can (and it is
567 a good idea to) overlap directly with autofocus area. Make sure neither drift nor autofocus area
568 overlap with an acquisition area.
569

570 NOTE: The template can be checked using the template execution function. This is a good idea
571 to see if acquisition areas need moving (e.g., too much/not enough carbon in images), but is not
572 necessary.

573

574 5.5.16. Go back to **Square selection**, and on the grid select the squares for acquisition. Use the
575 number of acquisition areas and expected data acquisition rate (from facility based on detectors
576 and experimental set up) to predict how many acquisition areas are required.

577

578 5.5.17. When all desired squares are selected, press **Prepare all Squares**.

579

580 5.5.18. Once each square is collected, navigate between the grid squares and fine tune the holes
581 using the **selection brush**.

582

583 5.6. Move to a stage location over specimen and use auto functions to set eucentric height.
584 Perform microscope alignments as previously described²⁸, but instead of performing Coma-free
585 alignment and correcting for objective astigmatism manually, make use of alignment tools within
586 the software. Briefly, set acquisition beam conditions, ensure the objective aperture (OA) is
587 removed and the stage is positioned over a beam stable area of specimen at eucentric height.
588 Perform coma-free alignment within the auto-functions before reinserting and centering the OA
589 and correcting the objective lens astigmatism with EPU. Ensure that both alignments converge
590 on suitable values (<150 nm of coma and close to zero astigmatism).

591

592 5.6.1. Before starting the automated acquisition run, ensure the autoloader turbo pump is
593 turned off, and the objective aperture is inserted.

594

595 5.7. In **Automated acquisition**, press **Start run** to commence automated data acquisition.

596

597 **6. Image processing to yield EM density map**

598

599 NOTE: The majority of cryoEM facilities offer pre-processing of micrograph movies 'on the fly'.
600 There are a wide variety of software packages and approaches available for this including RELION
601 pipelines^{28, 33}, cryoSPARC⁴³, Scipion³⁴ and WarpEM⁴⁴. A RELION based pipeline is described here
602 and it is assumed that the user has moved the micrograph movies to an appropriate storage
603 location with access to computing resources. An overview of the process and representative
604 results for a membrane protein project are provided, a detailed description and step by step
605 tutorial can be found on the RELION homepage: <https://www3.mrc-lmb.cam.ac.uk/relion>.

606

607 6.1. Perform 'on the fly' analysis of micrograph motion correction and CTF estimation. Start
608 RELION within the project directory. Schedule Import, Motion correction and CTF estimation jobs
609 to loop such that they are concurrent with data collection and transfer. A micrograph analysis
610 script²⁸ provides real-time visual feedback on astigmatism and estimated defocus values (see
611 representative results).

612

613 6.2. Pick particles from pre-processed micrographs. There are a number of automated particle
614 picking software packages to choose from. Reference free and template-based picking options
615 are available within the Auto-picking tab of RELION³⁷. Other programs may be used for various
616 steps, for example using crYOLO for particle picking³⁵.

617

618 6.3. Extract particles from the CTF-corrected micrographs.

619

620 NOTE: To reduce the computational time required for early, 'clean-up', processing steps, down-
621 scale/bin the particles upon extraction. Details on how run the extract job can be found in the
622 RELION 3.1 tutorial. For this project, particles were initially binned by a factor of 2.

623

624 6.4. Perform 2D class averaging. Classifying across 100-200 classes works well for most
625 datasets containing $\geq 100,000$ particles. It is not recommended to use many more than 200
626 classes or fewer than 50 classes, even where datasets are small unless the sample has high
627 symmetry (i.e., icosahedral virus) in which case fewer than 50 classes might still give a good
628 result. Set the mask diameter large enough to accommodate the longest dimension of the
629 particle, but tight enough to exclude any neighbouring particles (this may require some trial and
630 error).

631

632 6.5. Select good classes (i.e., those with structural details) using the subset selection job.
633 Examples of good and bad 2D class averages can be found in the representative results section.

634

635 6.6. Generate an initial model *de novo* from the data using the 3D initial model job in RELION.

636

637 NOTE: Less clean particle stacks may benefit from multi-reference *ab initio* SGD (stochastic
638 gradient descent) refinement since this provides an additional opportunity to sift out junk/sub-
639 optimal particles. Select a mask diameter that can accommodate the particle of interest, and
640 leave the default values for fields in the 'SGD' tab since these routinely perform well. Ensure that
641 the initial model looks reasonable in Chimera (or another appropriate visualisation program) (see
642 representative results).

643

644 6.7. Perform 3D classification to address heterogeneity in the data using the output from step
645 6.6 as a reference model. Assess the resulting maps in Chimera. Process particle stacks
646 corresponding to unique conformational states independently. Use the subset selection job to
647 select a class/classes of interest and generate particles.star files for the associated particle stacks.

648

649 6.8. Run 3D auto-refinement. Use the 3D class averages obtained in the previous step as
650 references for refinement of their corresponding particle stacks. If the resolution of the
651 refinement is approaching the Nyquist limit of the data, re-extract the particles without down-
652 scaling. After re-extraction, repeat the 3D auto-refine job with the unbinned particle stack. In this
653 case, the 3D reference models must be rescaled such that the pixel and box sizes are consistent
654 with those of the re-extracted particle images. Use the `relion_image_handler` command line tool
655 to carry out this operation.

656

657 6.9. Utilize symmetry in refinement if appropriate. If a reconstructed map possesses
658 symmetry, align the map on the appropriate symmetry axis using the `relion_align_symmetry`
659 command line tool. Use the resulting aligned map as a reference in a new 3D auto-refinement
660 job with the appropriate symmetry operator specified in the reference tab.

661
662 6.10. Sharpen maps from 3D auto-refinement. This is done using the post-processing job in
663 RELION, but first a suitable mask must be created from the refined map. The steps of mask
664 creation and post-processing are detailed in the RELION tutorial (see also representative results).
665

666 NOTE: The resolution of many reconstructions can be further improved using the Bayesian
667 polishing and CTF refinement functionalities in RELION. Use the CTF refinement job-type to
668 estimate and correct for higher order aberrations (beam tilt, trefoil aberrations and 4th order
669 aberrations) and, as separate jobs, anisotropic magnification and per-particle defocus. Following
670 this, use the Bayesian polishing job (trained or with default values) to address beam-induced
671 motion on a per-particle basis. As addressed in the RELION 3.1 tutorial, these jobs will likely
672 benefit from an iterative approach (CTF-refinement → Bayesian polishing → 3D auto-refinement
673 → post-processing → ...loop) since both benefit from higher resolution models.
674

675 6.11. Correct the handedness of EM density maps if necessary. Examine the maps to determine
676 whether the handedness is correct either by attempting to fit an existing atomic model, or
677 assessing the handedness of the alpha helical regions. Where required, flip the map along the z-
678 axis in UCSF Chimera⁴⁵ using the 'vop zflip' command.
679

680 **REPRESENTATIVE RESULTS:**

681 When screening, grids can be discarded at the atlas stage, where features resolved at low
682 magnification mark the grid as not suitable for data acquisition. For example, if a grid has been
683 subject to significant mechanical damage with the majority of grid squares broken (**Figure 2A**),
684 or where the grid appears to be 'dry', with no vitreous ice (**Figure 2B**). Such grids are typically
685 identifiable as the edges of the grid squares appear sharp and distinct. Across the majority of
686 grids made using the plunge freezing device, a gradient of ice is observed (**Figure 2C,D**). Particle
687 distribution, depending on the specimen of interest, can vary dramatically with ice thickness and
688 so screening a range of grid squares to assess particle distribution is recommended. Tools have
689 been implemented within EPU software during the atlas screening step to help the user identify
690 grid squares of similar or different ice thickness, which can be particularly useful to users who
691 are new to examining cryoEM grids (**Figure 2E, F**).
692

693 [Insert Figure 2 here]
694

695 When screening particle distribution, ensure that imaging parameters, such as magnification and
696 total electron dose, are similar to those expected to be used during data acquisition in order to
697 provide an accurate picture of expected results. During screening, an ideal particle distribution is
698 monodisperse with a range of particle orientations visible (depending on the specimen and
699 existing knowledge of the particle's morphology, this may be challenging to ascertain) (**Figure**
700 **3A**). The ice should be as thin as possible while accommodating the particles largest dimension,
701 if ice is too thin it can melt when illuminated with the electron beam. This causes excessive
702 motion in the micrograph, and areas that display this characteristic should be avoided (**Figure**
703 **3B**). From collective experience, this effect is most commonly observed when there is detergent
704 in the buffer. This can result in very thin ice at the centre of the hole and so particles can be

705 physically excluded and forced towards the edge. This effect is observed in **Figure 3C**, but in this
706 case it is not an extreme example and these images would still usefully contribute to a dataset.
707 Finally, the ice needs to be vitreous; exclude any areas of the grid (or grids) where the majority
708 or all of the images taken show crystalline ice (**Figure 3D**) from data acquisition. Often, non-
709 vitreous ice is observed at the edge of grid squares. Readers are referred to detailed reviews of
710 the variables that can be altered during grid vitrification¹⁶ and descriptions of particle behaviour
711 in the thin film environment^{46, 47} for further information.

712

713 [Insert Figure 3 here]

714

715 On-the-fly image processing can help to pick up errors and problems with data acquisition and
716 so is always recommended where possible. For example, excessive motion within micrographs
717 may indicate that the autoloader turbo pump is active, or data is being collected on a cracked
718 grid square where ice is moving significantly in the electron beam, indicating the grid square
719 should be skipped. On the fly CTF estimation can reveal circumstances where a positive focus
720 point (rather than defocus) is applied (where CTF estimation programs and parameters to find
721 these points are used), and determine the phase shift where a Volta phase plate⁴⁸ is used. On the
722 fly image processing pipelines often include a graphical summary of the data (**Figure 4A**) to make
723 it easier for users to assess micrograph quality quickly and decide if data collection amendments
724 are required.

725

726 Selection of particles from micrographs, whilst avoiding ‘false positives’ such as contamination
727 or the grid support film can require optimisation. However, particle pickers such as crYOLO often
728 work sufficiently well using default parameters for a ‘first pass’ of the data (**Figure 4B**), enabling
729 progression to 2D class averaging where it can be easier to assess the quality of the data and the
730 likelihood of downstream success. For most projects, 2D classification of $\sim > 10k$ particles should
731 start to reveal classes which have secondary structure detail. To proceed to 3D, the 2D
732 classification stage should typically reveal classes representing a range of particle orientations. If
733 a preferred orientation is revealed, more iterations of sample preparation¹⁶ or further data
734 acquisition with the sample tilted may be required⁴⁹. All classes which show secondary structure
735 detail should be chosen to take forward to 3D analysis, while ‘junk’ particles are discarded (**Figure**
736 **4C**).

737

738 [Insert Figure 4 here]

739

740 A small subset of particles can be used to generate an initial model (**Figure 5A**). This initial model
741 can then be used as a starting model in 3D classification and refinement. In the case of RagAB,
742 the dataset contained three distinct conformers which can be separated during 3D classification
743 (**Figure 5B**). Particles contributing to each of these classes can then be treated independently and
744 used to refine an EM density map which can then be subject to further interpretation and model
745 building.

746

747 [Insert Figure 5 here]

748

749 **FIGURE AND TABLE LEGENDS:**

750

751 **Figure 1: Cumulative submissions to the EMDB from 2012 to December 2020.**

752

753 **Figure 2: Example low magnification ‘atlas’ montages from screening sessions.** **A)** A grid which
754 has suffered significant damage with the majority of grid squares broken – unsuitable for
755 collection. **B)** A dry grid with no vitreous ice – unsuitable for collection. **C)** A grid demonstrating
756 an ice gradient with ~ 50% of the grid useable. **D)** An ice gradient with ~ 33% of the grid useable.
757 Both **C** and **D**, are suitable for data collection if the usable grid squares have an ice thickness
758 appropriate for collection, and there are enough acquisition areas to satisfy the minimum
759 duration of a collection (e.g., 24 h) **E)** An example atlas with range of ice thicknesses. **F)** The same
760 atlas presented in E but with, grid squares categorized and coloured by EPU software according
761 to ice thickness.

762

763 **Figure 3: Representative micrographs showing differing particle distributions.** **A)** An ‘ideal’
764 distribution of monodisperse particles adopting a range of orientations. **B)** Overly thin ice in the
765 middle of the hole that it deforms upon exposure to the electron beam causing excessive motion
766 in the micrograph. This effect is most often observed when detergent is present in the buffer **C)**
767 Where ice is thinner in the centre of the hole, this physically excludes particles from the centre,
768 causing crowding of particles towards the hole edge. In this case it is not extreme enough to
769 prevent these images being useful, but it suggests it is worth screening slightly thicker areas. **D)**
770 Ice is not vitreous, data should not be collected on areas which look like this example micrograph.

771

772 **Figure 4: Initial image processing steps.** **A)** Output from an ‘on the fly’ image processing script.
773 **B)** Example micrograph (left) with appropriately auto-picked particles identified using the crYOLO
774 general model (right, with particles bounded by red squares) Scale bars (white) are 50 nm. **C)**
775 Results from 2D classification showing classes which were discarded in the red square, and
776 classes from which particles were selected for further processing in green.

777

778 **Figure 5: Generating 3D EM density map.** **A)** Typical initial model generated using RELION. **B)** 3D
779 classification over 5 classes showing separation of particles into three distinct conformational
780 states: open-open (green), open-closed (blue), closed-closed (purple). **C)** Process of mask
781 creation. The map from 3D refinement (left) should be visualized in chimera. The volume viewer
782 can then be used to identify the lowest threshold at which the map is free from disjointed, noisy
783 density (middle). This threshold value is input as initial binarization threshold in the RELION Mask
784 creation job. An example mask output is shown in grey (right). **D)** High resolution EM density map
785 of the open-closed state of RagAB (EMD-10245), filtered and colored by local resolution (Å).

786

787 **DISCUSSION:**

788 In this protocol we have described a basic pipeline applicable to specimens amenable to routine
789 SPA. While this filter paper blotting method of thin film formation and vitrification is undoubtedly
790 successful given its use in the vast majority of SPA projects to date, it comes with a number of
791 disadvantages. These include sample wastage, the slow timescales (seconds) required to form
792 the thin film and freeze the specimen, reported irreproducibility²⁷ and reported negative effects

793 of using filter paper to blot away excess liquid⁵⁰. Recently, new technologies have been
794 developed to improve reproducibility of thin film production^{51, 52}. Other technologies have been
795 developed which reduce the time between sample application and vitrification⁵³⁻⁵⁵. While filter
796 paper-based methods for thin film formation remain most ubiquitous method of SPA cryoEM
797 sample preparation at the time of writing, these new technologies may bring a range of benefits
798 in terms of efficiency and reproducibility of grid vitrification, as well as creating new opportunities
799 to bring in additional experimental dimensions, such as time resolution and rapid mixing prior to
800 vitrification.

801

802 The process of grid screening for most users is presently a qualitative process which involves the
803 acquisition of low magnification atlases followed by taking high-magnification images across the
804 grid to assess particle distribution. While this is a sufficiently robust approach for some types of
805 specimen, it can be difficult to assess by eye if the specimen is indeed what the researcher is
806 hoping to image or has a preferred orientation, for example with small (<200 kDa) samples or
807 where the low-resolution morphology makes it hard to identify by eye if a range of particle
808 distributions are present. For some projects, it is impossible to determine if the specimen is as
809 desired, for example where a ligand is bound or where the sample is being screened to assess if
810 a small (e.g., 10 kDa) subunit is still present in association with a complex. For these projects, fully
811 automated pipelines for data analysis combined with a 'short' 0.5 – 1-h collections, that can
812 proceed through image processing steps to 2D classification or even 3D classification and
813 refinement would help efficiently determine if a longer collection is warranted. These pipelines
814 are still under development and are not widely implemented at present, but they have the
815 potential to improve the efficiency of cryoEM grid screening, especially for challenging
816 specimens.

817

818 Improvements in direct electron detectors, as well as modifications in microscopy combined with
819 advances in image processing such as image shift data collection, have increased the throughput
820 and quality of images produced during data acquisition. This increase in the rate of data being
821 collected highlights the need for thorough screening of cryoEM grids ahead of many TB of data
822 being acquired.

823

824 CryoEM SPA has become a truly mainstream structural biology technique, and in many cases the
825 'go to' approach for some classes of specimens, such as heterogeneous and labile
826 macromolecular complexes. While the protocol here describes a basic overview of the SPA
827 pipeline, each section covered here (grid vitrification and screening, cryoEM and image
828 processing) is a topic in its own right and worthy of exploration during the development of an
829 SPA project. As sample preparation and microscopy technologies progress, and new image
830 processing algorithms and approaches come online, SPA will continue to develop as a pipeline,
831 assisting researchers in gaining insight into complex biological systems.

832

833 **ACKNOWLEDGMENTS:**

834 J B. R. White is funded by the Wellcome Trust (215064/Z/18/Z). The FEI Titan Krios microscopes
835 were funded by the University of Leeds (UoL ABSL award) and Wellcome Trust (108466/Z/15/Z).
836 We thank M Iadanza for use of his micrograph analysis script. We acknowledge Diamond Light

837 Source for access and support of the cryo-EM facilities at the UK's national Electron Bio-imaging
838 Centre (eBIC) funded by the Wellcome Trust, MRC and BBRSC.

839

840 **DISCLOSURES:**

841 No conflicts of interest are reported.

842

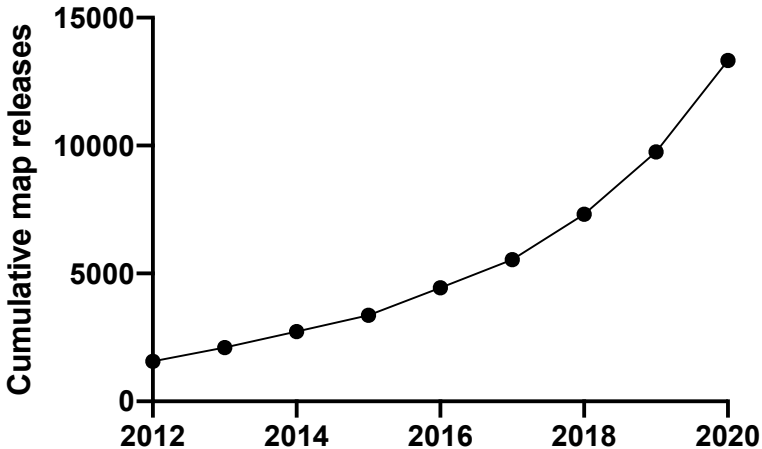
843 **REFERENCES:**

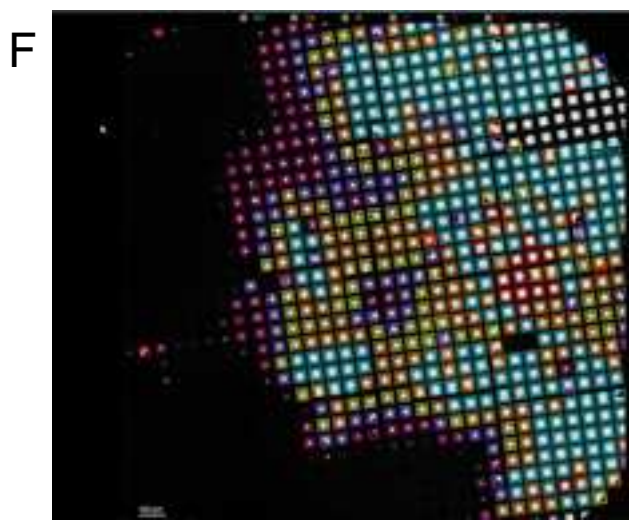
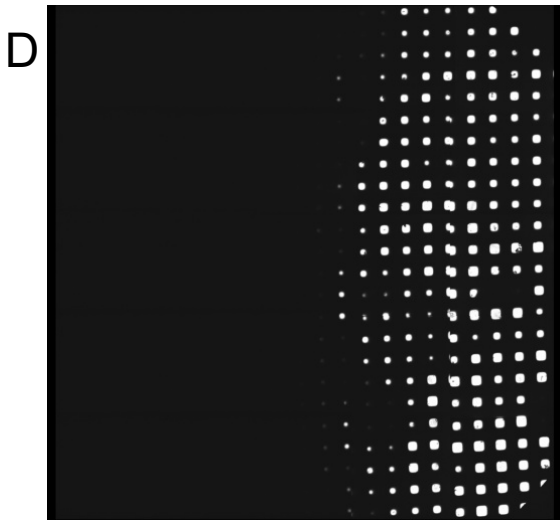
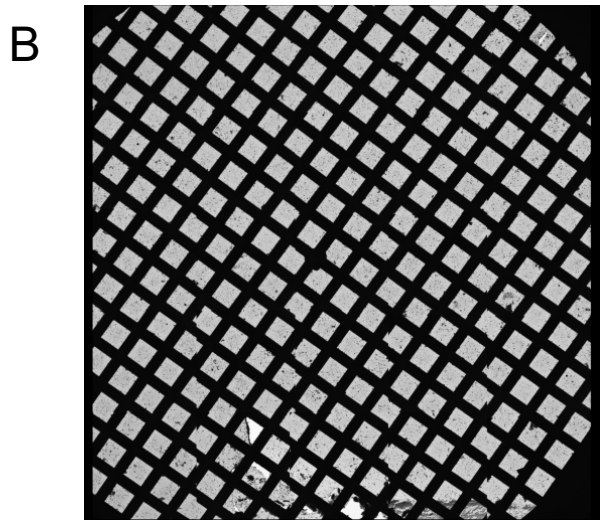
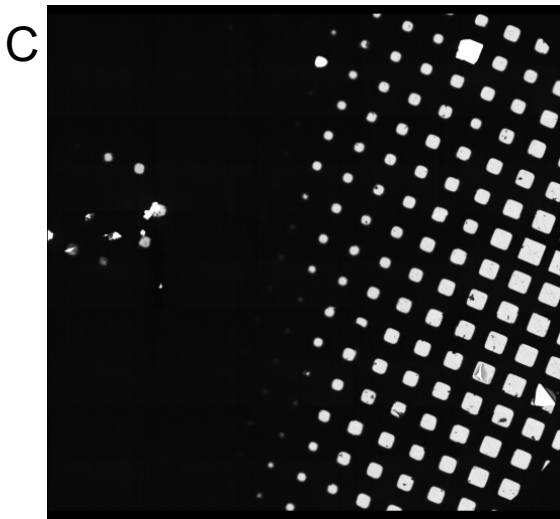
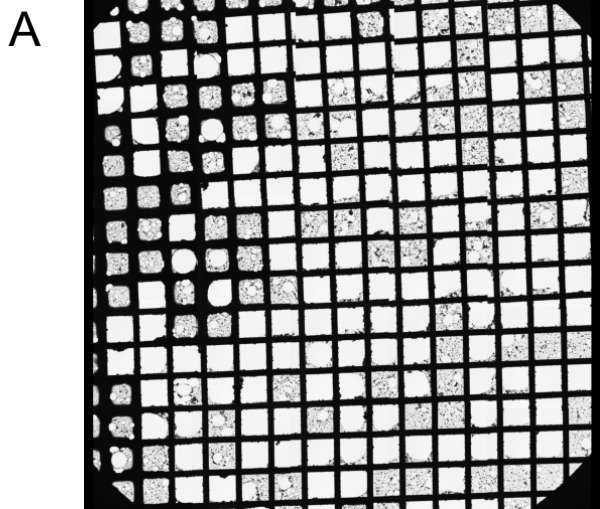
- 844 1. Kuehlbrandt, W. The Resolution Revolution. *Science*. **343** (6178), 1443–1444, doi:
845 10.1126/science.1251652 (2014).
- 846 2. McMullan, G., Faruqi, A.R., Henderson, R. Direct Electron Detectors. *Methods in*
847 *Enzymology*. doi: 10.1016/bs.mie.2016.05.056 (2016).
- 848 3. Elmlund, D., Le, S.N., Elmlund, H. High-resolution cryo-EM: the nuts and bolts. *Current*
849 *Opinion in Structural Biology*. doi: 10.1016/j.sbi.2017.03.003 (2017).
- 850 4. Lyumkis, D. Challenges and opportunities in cryo-EM single-particle analysis. *Journal of*
851 *Biological Chemistry*. doi: 10.1074/jbc.REV118.005602 (2019).
- 852 5. Nakane, T. *et al.* Single-particle cryo-EM at atomic resolution. *Nature*. doi:
853 10.1038/s41586-020-2829-0 (2020).
- 854 6. Yip, K.M., Fischer, N., Paknia, E., Chari, A., Stark, H. Atomic-resolution protein structure
855 determination by cryo-EM. *Nature*. doi: 10.1038/s41586-020-2833-4 (2020).
- 856 7. Conley, M.J. *et al.* Calicivirus VP2 forms a portal-like assembly following receptor
857 engagement. *Nature*. **565** (7739), 377–381, at <[https://doi.org/10.1038/s41586-018-](https://doi.org/10.1038/s41586-018-0852-1)
858 [0852-1](https://doi.org/10.1038/s41586-018-0852-1)> (2019).
- 859 8. Hesketh, E.L. *et al.* The 3.3 Å structure of a plant geminivirus using cryo-EM. *Nature*
860 *communications*. **9** (1), 2369, at <<https://doi.org/10.1038/s41467-018-04793-6>> (2018).
- 861 9. Malone, L.A. *et al.* Cryo-EM structure of the spinach cytochrome b6 f complex at 3.6 Å
862 resolution. *Nature*. **575** (7783), 535–539, doi: 10.1038/s41586-019-1746-6 (2019).
- 863 10. Madej, M. *et al.* Structural and functional insights into oligopeptide acquisition by the
864 RagAB transporter from *Porphyromonas gingivalis*. *Nature Microbiology*. doi:
865 10.1038/s41564-020-0716-y (2020).
- 866 11. Gallardo, R. *et al.* Fibril structures of diabetes-related amylin variants reveal a basis for
867 surface-templated assembly. *Nature Structural and Molecular Biology*. doi:
868 10.1038/s41594-020-0496-3 (2020).
- 869 12. Scarff, C. *et al.* Structure of the shutdown state of myosin-2. *Nature*. doi: 10.1038/s41586-
870 020-2990-5 (2020).
- 871 13. Scarff, C.A. *et al.* Structure of the protective nematode protease complex H-gal-GP and its
872 conservation across roundworm parasites. *PLoS Pathogens*. **16** (4), e1008465 (2020).
- 873 14. Wu, M., Lander, G.C. How low can we go? Structure determination of small biological
874 complexes using single-particle cryo-EM. *Current Opinion in Structural Biology*. doi:
875 10.1016/j.sbi.2020.05.007 (2020).
- 876 15. Khoshouei, M., Radjainia, M., Baumeister, W., Danev, R. Cryo-EM structure of
877 haemoglobin at 3.2 Å determined with the Volta phase plate. *Nature Communications*. doi:
878 10.1038/ncomms16099 (2017).
- 879 16. Drulyte, I. *et al.* Approaches to altering particle distributions in cryo-electron microscopy
880 sample preparation. *Acta crystallographica. Section D, Structural biology*. **74** (Pt 6), 560–

- 881 571, doi: 10.1107/S2059798318006496 (2018).
- 882 17. Thompson, R.F., Walker, M., Siebert, C.A., Muench, S.P., Ranson, N.A. An introduction to
883 sample preparation and imaging by cryo-electron microscopy for structural biology.
884 *Methods*. **100**, 3–15 (2016).
- 885 18. Cheng, Y., Grigorieff, N., Penczek, P.A., Walz, T. A primer to single-particle cryo-electron
886 microscopy. *Cell*. **161** (3), 438–449, doi: 10.1016/j.cell.2015.03.050 (2015).
- 887 19. Scarff, C.A., Fuller, M.J.G., Thompson, R.F., Iadanza, M.G. Variations on negative stain
888 electron microscopy methods: tools for tackling challenging systems. *JoVE (Journal of*
889 *Visualized Experiments)*. (132), e57199 (2018).
- 890 20. Ohi, M., Li, Y., Cheng, Y., Walz, T. Negative Staining and Image Classification - Powerful
891 Tools in Modern Electron Microscopy. *Biological procedures online*. **6**, 23–34, doi:
892 10.1251/bpo70 (2004).
- 893 21. Baker, L.A., Rubinstein, J.L. Radiation Damage in Electron Cryomicroscopy. *Methods in*
894 *enzymology*. **481**, 371–388, doi: 10.1016/S0076-6879(10)81015-8 (2010).
- 895 22. Dubochet, J. *et al.* Cryo-electron microscopy of vitrified specimens. *Quarterly Reviews of*
896 *Biophysics*. **21** (02), 129–228, doi: 10.1017/S0033583500004297 (1988).
- 897 23. Passmore, L.A., Russo, C.J. Specimen Preparation for High-Resolution Cryo-EM. *Methods*
898 *in enzymology*. **579**, 51–86, doi: 10.1016/bs.mie.2016.04.011 (2016).
- 899 24. Sgro, G.G., Biosciences, T.R.D.C.F. in M., 2018 Cryo-EM grid preparation of membrane
900 protein samples for single particle analysis. *researchgate.net*. at
901 <[https://www.researchgate.net/profile/Tiago_Costa12/publication/326710861_Cryo-](https://www.researchgate.net/profile/Tiago_Costa12/publication/326710861_Cryo-EM_Grid_Preparation_of_Membrane_Protein_Samples_for_Single_Particle_Analysis/links/5b602bd6aca272a2d676aec2/Cryo-EM-Grid-Preparation-of-Membrane-Protein-Samples-for-Single-Parti)
902 [EM_Grid_Preparation_of_Membrane_Protein_Samples_for_Single_Particle_Analysis/lin](https://www.researchgate.net/profile/Tiago_Costa12/publication/326710861_Cryo-EM_Grid_Preparation_of_Membrane_Protein_Samples_for_Single_Particle_Analysis/links/5b602bd6aca272a2d676aec2/Cryo-EM-Grid-Preparation-of-Membrane-Protein-Samples-for-Single-Parti)
903 [ks/5b602bd6aca272a2d676aec2/Cryo-EM-Grid-Preparation-of-Membrane-Protein-](https://www.researchgate.net/profile/Tiago_Costa12/publication/326710861_Cryo-EM_Grid_Preparation_of_Membrane_Protein_Samples_for_Single_Particle_Analysis/links/5b602bd6aca272a2d676aec2/Cryo-EM-Grid-Preparation-of-Membrane-Protein-Samples-for-Single-Parti)
904 [Samples-for-Single-Parti](https://www.researchgate.net/profile/Tiago_Costa12/publication/326710861_Cryo-EM_Grid_Preparation_of_Membrane_Protein_Samples_for_Single_Particle_Analysis/links/5b602bd6aca272a2d676aec2/Cryo-EM-Grid-Preparation-of-Membrane-Protein-Samples-for-Single-Parti)>.
- 905 25. Naydenova, K., Jia, P., Russo, C.J. Cryo-EM with sub–1 Å specimen movement. *Science*. doi:
906 10.1126/science.abb7927 (2020).
- 907 26. Passmore, L.A., Russo, C.J. Specimen Preparation for High-Resolution Cryo-EM. *Methods*
908 *in Enzymology*. doi: 10.1016/bs.mie.2016.04.011 (2016).
- 909 27. Carragher, B. *et al.* Current outcomes when optimizing ‘standard’ sample preparation for
910 single-particle cryo-EM. *Journal of Microscopy*. doi: 10.1111/jmi.12834 (2019).
- 911 28. Thompson, R.F., Iadanza, M.G., Hesketh, E.L., Rawson, S., Ranson, N.A. Collection, pre-
912 processing and on-the-fly analysis of data for high-resolution, single-particle cryo-electron
913 microscopy. *Nature protocols*. **14** (1), 100–118 (2019).
- 914 29. Suloway, C. *et al.* Automated molecular microscopy: the new Legimon system. *Journal of*
915 *Structural Biology*. **151** (1), 41–60, doi: 10.1016/j.jsb.2005.03.010 (2005).
- 916 30. Zhang, J. *et al.* JADAS: A customizable automated data acquisition system and its
917 application to ice-embedded single particles. *Journal of Structural Biology*. doi:
918 10.1016/j.jsb.2008.09.006 (2009).
- 919 31. Mastronarde, D.N. SerialEM: A program for automated tilt series acquisition on Tecnai
920 microscopes using prediction of specimen position. *Microscopy and Microanalysis*. doi:
921 10.1017/s1431927603445911 (2003).
- 922 32. Schorb, M., Haberbosch, I., Hagen, W.J.H., Schwab, Y., Mastronarde, D.N. Software tools
923 for automated transmission electron microscopy. *Nature Methods*. doi: 10.1038/s41592-
924 019-0396-9 (2019).

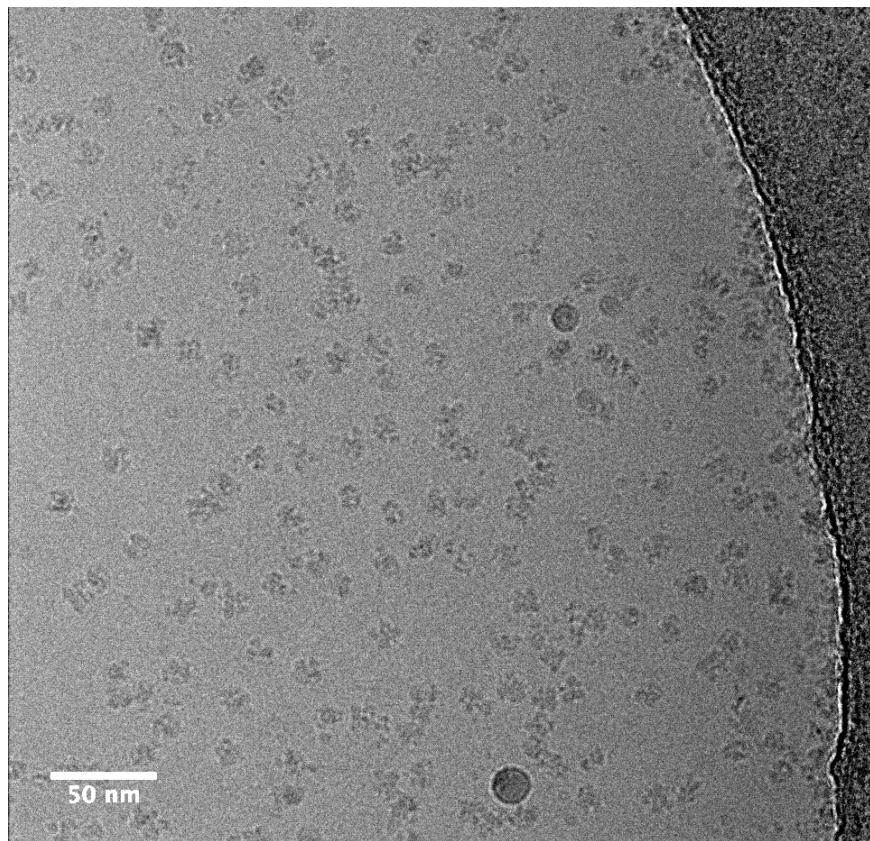
- 925 33. Fernandez-Leiro, R., Scheres, S.H.W. A pipeline approach to single-particle processing in
926 RELION. *Acta crystallographica. Section D, Structural biology*. **73** (Pt 6), 496–502, doi:
927 10.1107/S2059798316019276 (2017).
- 928 34. Gómez-Blanco, J. *et al.* Using Scipion for stream image processing at Cryo-EM facilities.
929 *Journal of Structural Biology*. doi: 10.1016/j.jsb.2018.10.001 (2018).
- 930 35. Wagner, T. *et al.* SPHIRE-crYOLO is a fast and accurate fully automated particle picker for
931 cryo-EM. *Communications biology*. **2** (1), 213–218, doi: 10.1038/s42003-019-0437-z
932 (2019).
- 933 36. Bepler, T. *et al.* TOPAZ: A Positive-Unlabeled Convolutional Neural Network CryoEM
934 Particle Picker that can Pick Any Size and Shape Particle. *Microscopy and Microanalysis*.
935 doi: 10.1017/s143192761900566x (2019).
- 936 37. Zivanov, J. *et al.* New tools for automated high-resolution cryo-EM structure
937 determination in RELION-3. *eLife*. **7**, 163, doi: 10.7554/eLife.42166 (2018).
- 938 38. Zivanov, J., Nakane, T., Scheres, S.H.W. A Bayesian approach to beam-induced motion
939 correction in cryo-EM single-particle analysis. *IUCrJ*. doi: 10.1107/S205225251801463X
940 (2019).
- 941 39. Cianfrocco, M.A., Kellogg, E.H. What Could Go Wrong? A Practical Guide to Single-Particle
942 Cryo-EM: From Biochemistry to Atomic Models. *Journal of Chemical Information and*
943 *Modeling*. doi: 10.1021/acs.jcim.9b01178 (2020).
- 944 40. Tagari, M., Newman, R., Chagoyen, M., Carazo, J.M., Henrick, K. New electron microscopy
945 database and deposition system. *Trends in Biochemical Sciences*. doi: 10.1016/S0968-
946 0004(02)02176-X (2002).
- 947 41. Berman, H.M. *et al.* The Protein Data Bank. *Nucleic Acids Research*. doi:
948 10.1093/nar/28.1.235 (2000).
- 949 42. Ludin, A., Korir, P.K., Salavert-Torres, J., Kleywegt, G.J., Patwardhan, A. EMPIAR: A public
950 archive for raw electron microscopy image data. *Nature Methods*. doi:
951 10.1038/nmeth.3806 (2016).
- 952 43. Punjani, A., Rubinstein, J.L., Fleet, D.J., Brubaker, M.A. CryoSPARC: Algorithms for rapid
953 unsupervised cryo-EM structure determination. *Nature Methods*. doi:
954 10.1038/nmeth.4169 (2017).
- 955 44. Tegunov, D., Cramer, P. Real-time cryo-electron microscopy data preprocessing with
956 Warp. *Nature Methods*. doi: 10.1038/s41592-019-0580-y (2019).
- 957 45. Goddard, T.D. *et al.* UCSF ChimeraX: Meeting modern challenges in visualization and
958 analysis. *Protein Science*. **27** (1), 14–25, doi: 10.1002/pro.3235 (2018).
- 959 46. Klebl, D.P. *et al.* Need for Speed: Examining Protein Behavior during CryoEM Grid
960 Preparation at Different Timescales. *Structure*. doi: 10.1016/j.str.2020.07.018 (2020).
- 961 47. Noble, A.J. *et al.* Routine single particle CryoEM sample and grid characterization by
962 tomography. *eLife*. **7**, 32, doi: 10.7554/eLife.34257 (2018).
- 963 48. Danev, R., Buijsse, B., Khoshouei, M., Plitzko, J.M., Baumeister, W. Volta potential phase
964 plate for in-focus phase contrast transmission electron microscopy. *Proceedings of the*
965 *National Academy of Sciences*. doi: 10.1073/pnas.1418377111 (2014).
- 966 49. Zi Tan, Y. *et al.* Addressing preferred specimen orientation in single-particle cryo-EM
967 through tilting. *Nature Methods*. doi: 10.1038/nmeth.4347 (2017).
- 968 50. Armstrong, M., Han, B.-G., Gomez, S., Turner, J., Fletcher, D.A., Glaeser, R.M. Microscale

- 969 Fluid Behavior during Cryo-EM Sample Blotting. *Biophysical Journal*. **118** (3), 708–719, doi:
970 10.1016/j.bpj.2019.12.017 (2020).
- 971 51. Arnold, S.A. *et al.* Blotting-free and lossless cryo-electron microscopy grid preparation
972 from nanoliter-sized protein samples and single-cell extracts. *Journal of Structural Biology*.
973 doi: 10.1016/j.jsb.2016.11.002 (2017).
- 974 52. Dandey, V.P. *et al.* Spotiton: New Features and Applications. *Journal of Structural Biology*.
975 doi: 10.1016/j.jsb.2018.01.002 (2018).
- 976 53. Rubinstein, J.L. *et al.* Shake-it-off: a simple ultrasonic cryo-EM specimen-preparation
977 device. *Acta crystallographica. Section D, Structural biology*. **75** (Pt 12), 1063–1070, doi:
978 10.1107/S2059798319014372 (2019).
- 979 54. Tan, Y.Z., Rubinstein, J.L. Through-grid wicking enables high-speed cryoEM specimen
980 preparation. *bioRxiv*. doi: 10.1101/2020.05.03.075366 (2020).
- 981 55. Klebl, D.P. *et al.* Sample deposition onto cryo-EM grids: From sprays to jets and back. *Acta*
982 *Crystallographica Section D: Structural Biology*. doi: 10.1107/S2059798320002958 (2020).
983

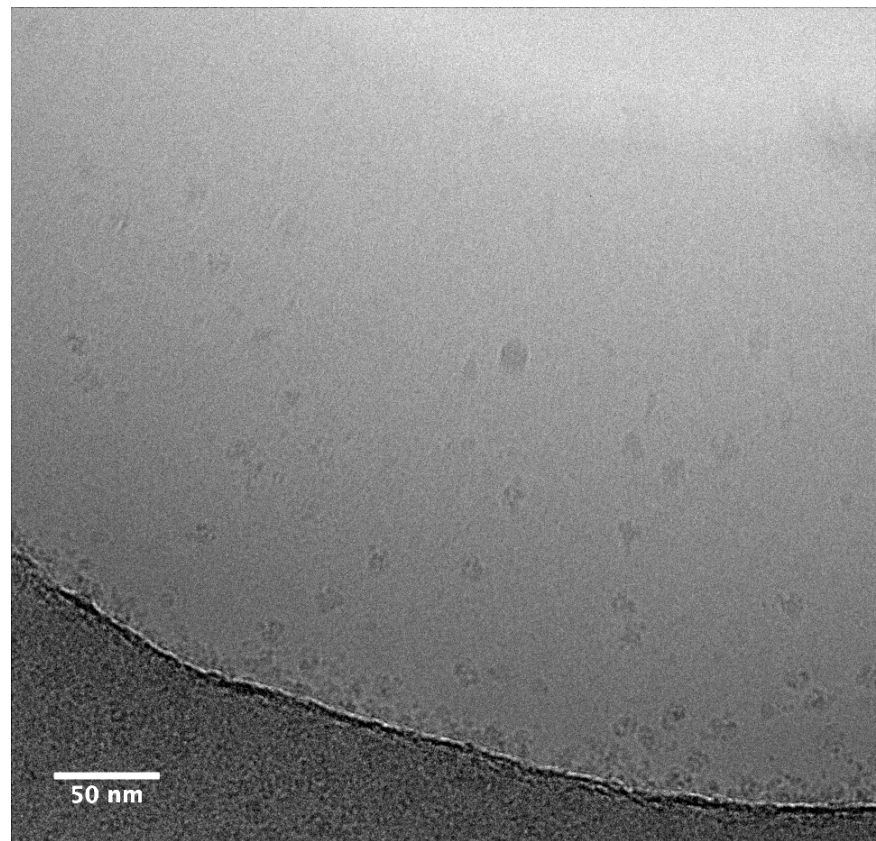




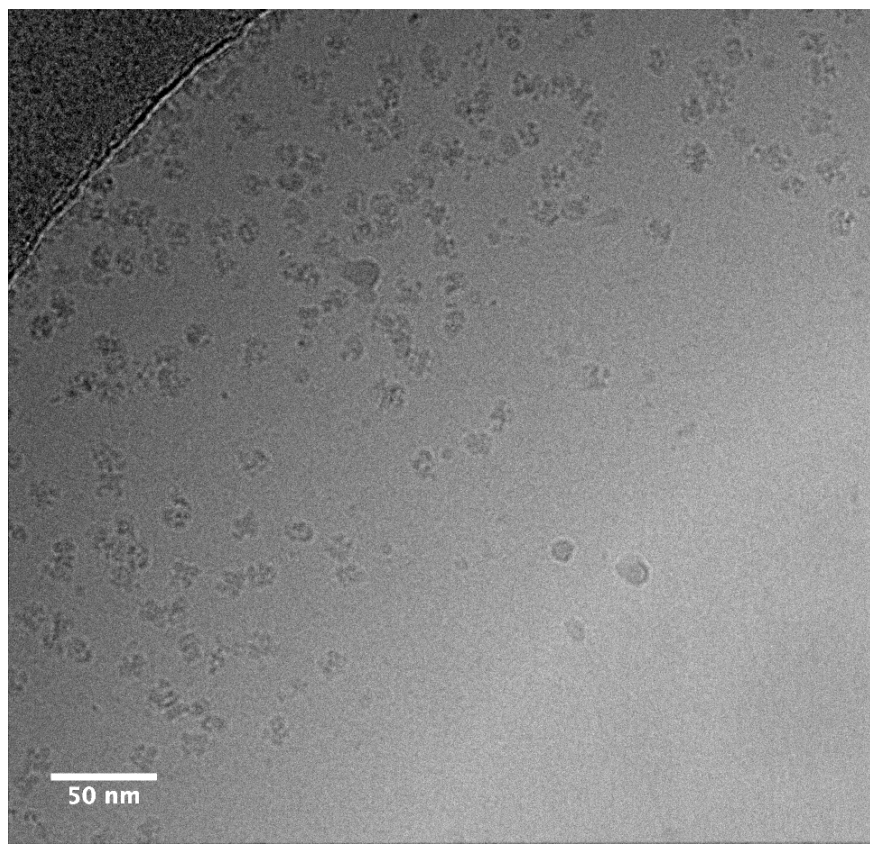
A



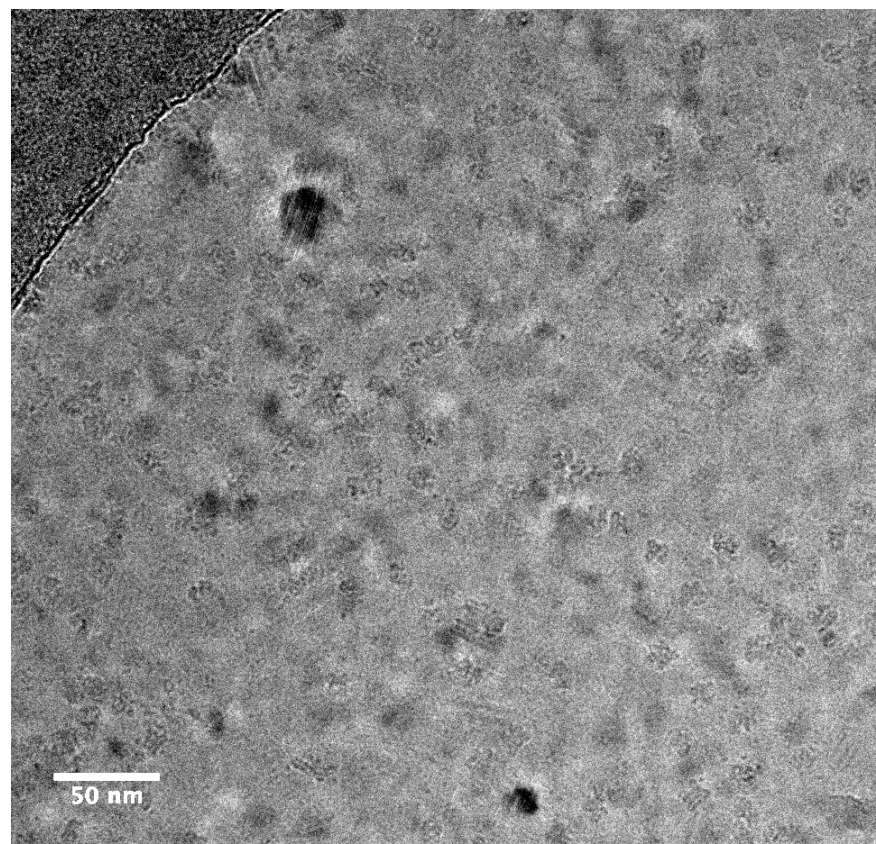
B

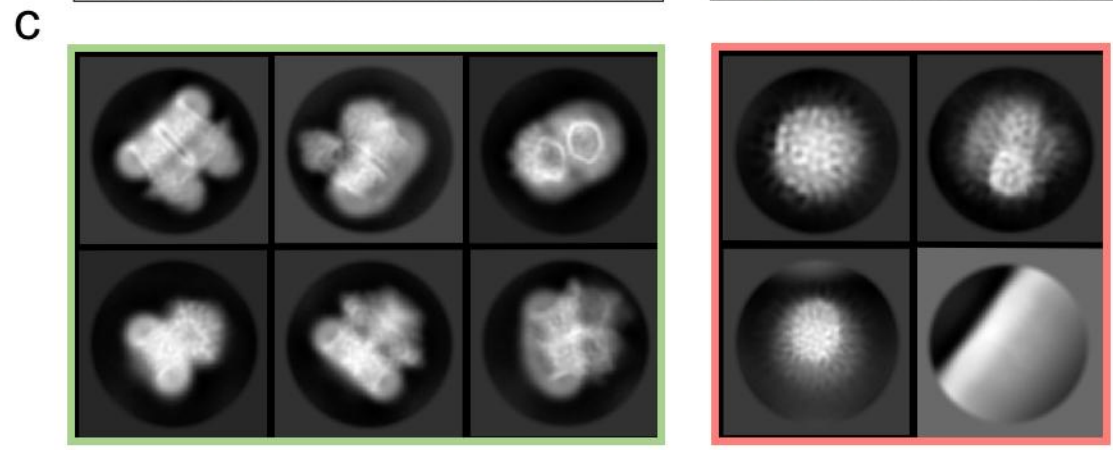
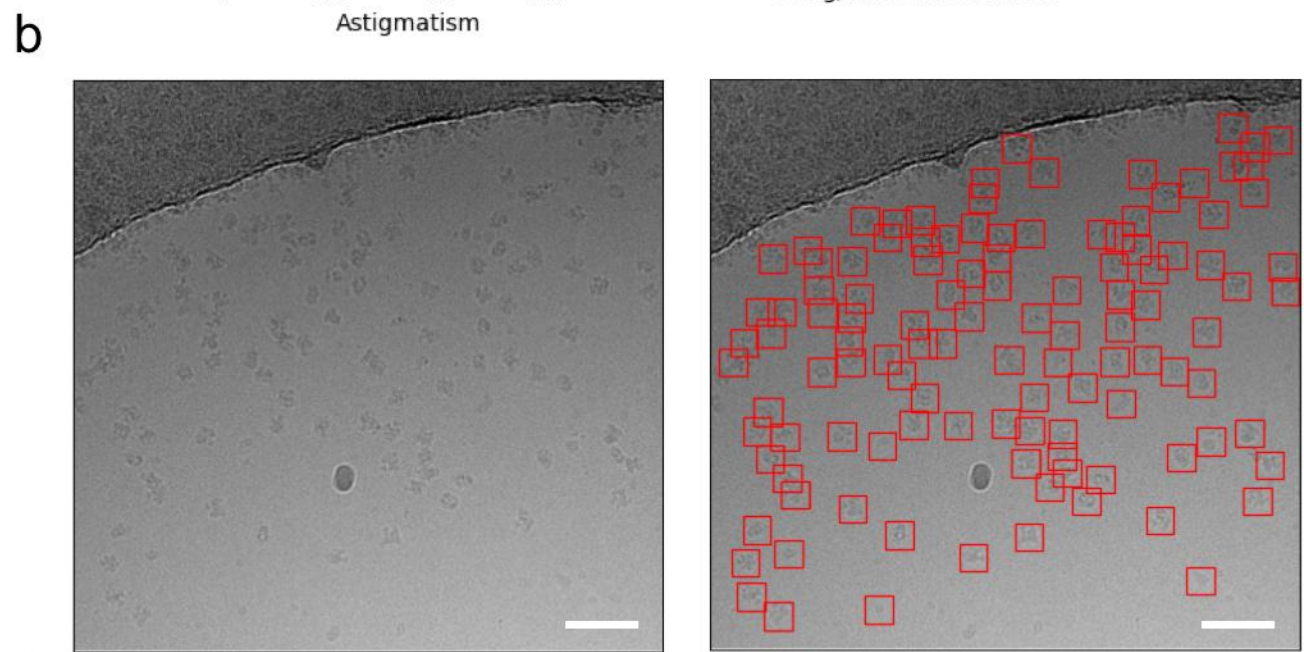
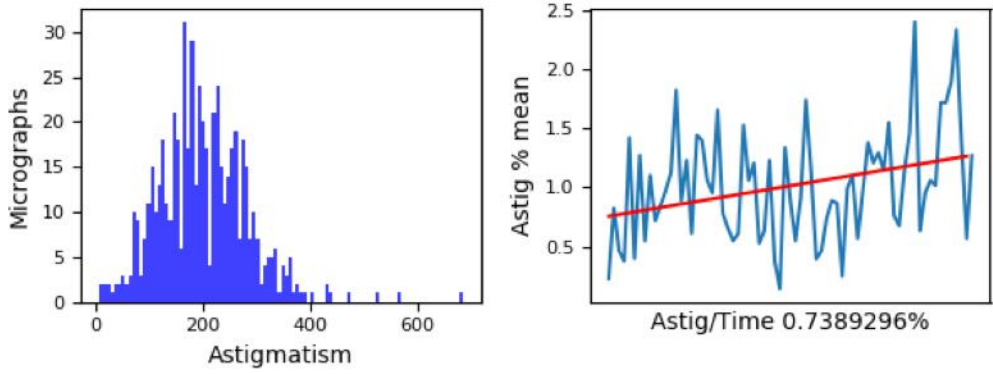
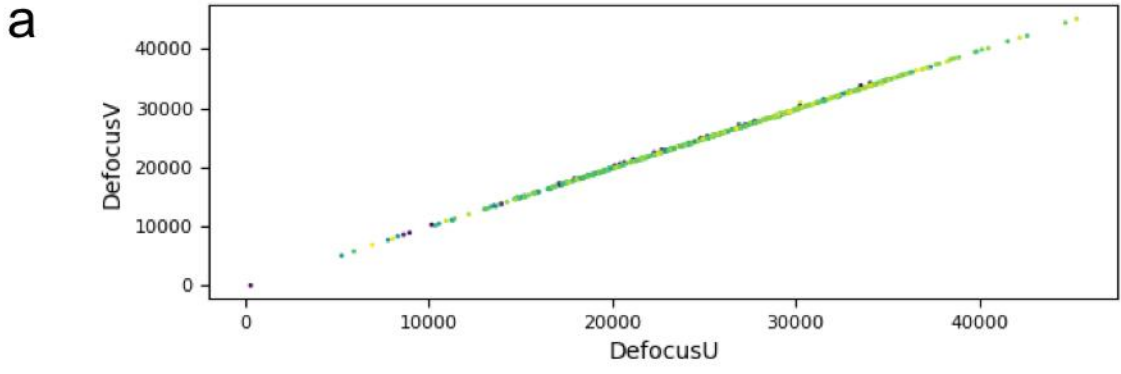


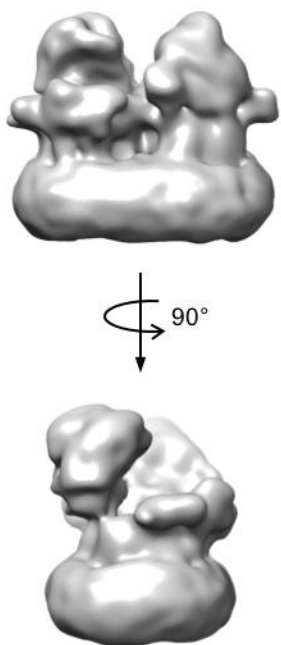
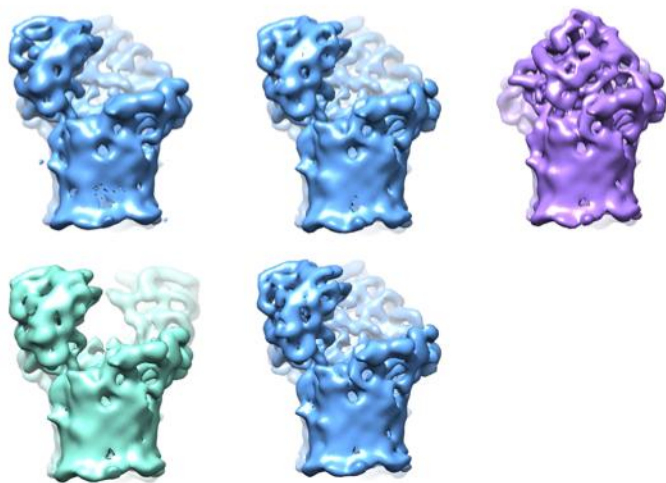
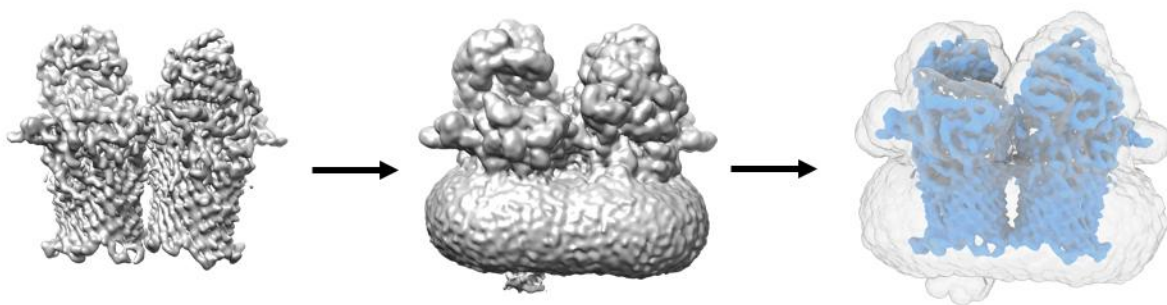
C



D





a**b****c****d**